LETTER

A compact spectrum splitting concentrator for high concentration photovoltaics based on the dispersion of a lens

IOP Publishing
Letters
Journal of Optics
J. Opt. **20** (2018) 06LT01 (8pp)
https://doi.org/10.1088/2040-8986/aabbf0

Letter

A compact spectrum splitting concentrator for high concentration photovoltaics based on the dispersion of a lens

J He[1], C A Flowers[2], Y Yao[1], H A Atwater[2], A A Rockett[3] and R G Nuzzo[1]

[1] Department of Chemistry and Frederick Seitz Materials Research Laboratory, University of Illinois at Urbana-Champaign, Urbana, IL, 61801, United States of America
[2] Thomas J. Watson Laboratories of Applied Physics, California Institute of Technology, Pasadena, CA 91125, United States of America
[3] George S. Ansell Department of Metallurgical and Materials Engineering, Colorado School of Mines, Golden, CO 80401, United States of America

E-mail: r-nuzzo@illinois.edu

Received 19 February 2018, revised 27 March 2018
Accepted for publication 5 April 2018
Published 30 April 2018

Abstract

Photovoltaic devices used in conjunction with functional optical elements for light concentration and spectrum splitting are known to be a viable approach for highly efficient photovoltaics. Conventional designs employ discrete optical elements, each with the task of either performing optical concentration or separating the solar spectrum. In the present work, we examine the performance of a compact photovoltaic architecture in which a single lens plays a dual role as both a concentrator and a spectrum splitter, the latter made possible by exploiting its intrinsic dispersion. A four-terminal two-junction InGaP/GaAs device is prepared to validate the concept and illustrates pathways for improvements. A spectral separation in the visible range is demonstrated at the focal point of a plano-convex lens with a geometric concentration ratio of 1104X with respect to the InGaP subcell.

Supplementary material for this article is available online

Keywords: spectrum splitting, high concentration photovoltaics, lens, dispersion

Introduction

The concentration of solar radiation for use with photovoltaics has been extensively studied due to the fact that the efficiencies of these devices increase logarithmically with light intensity, thus representing a significant pathway through which to realize improvements in performance. Perhaps as importantly, high concentration ratios potentially allow the use of more expensive but higher performance materials or difficult-to-produce photovoltaic device designs. One notable example is the use of multijunction (MJ) solar cells [1], which employ multiple bandgaps for broad spectrum absorption and reduced thermalization losses. A classic theoretical study, for example, shows that such devices can achieve efficiencies up to 85% with an infinite number of junctions [2]. While it is impossible to have an infinite number of junctions, studies have been reported on systems reaching very high efficiencies by employing three or more different subcells [3–5]. These solar cells are typically made from III–V semiconductor alloys (such as GaInP, GaAs and InP) whose bandgaps can be easily tailored by alloy composition tuning [6]. With progress in understanding and perfecting solar cell device physics [7, 8] along with improving upon the optical performance of solar cells [9–11], it is now possible to create MJ solar cells with a record cell efficiency of 46% (GaInP/GaAs; GaInAsP/GaInAs, 508X) that further illustrate realistic pathways to the 50% milestone [12, 13].

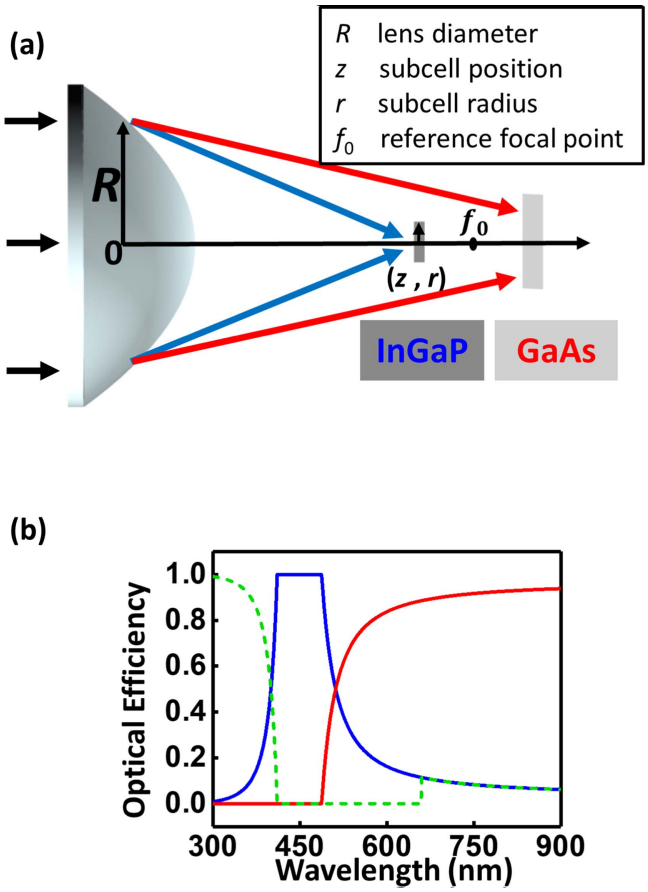

Figure 1. (a) Schematic illustration of the concentrator architecture. 'Blue photons' fall onto the InGaP subcell closer to the lens, while 'red' photons pass by the edges of the InGaP subcell and fall onto the GaAs subcell. The InGaP subcell with a radius r is placed at z on the optical axis whilst GaAs subcell is placed further along the optical axis such that it is large enough to collect all the rays that have a focal length $>z$ and which pass by the InGaP subcell. (b) A numerical example of the optical efficiencies of the InGaP subcell (blue) and GaAs subcell (red) for a lens made with dense flint glass (SF5), with an InGaP subcell position $z/f_0 = 0.9637$ and geometric concentration ratio $R^2/r^2 = 4289$. Optical loss (green dashed line) is found at the two ends of the InGaP subcell absorption window.

The MJ devices used in concentrating systems are typically monolithically-integrated tandem stacks epitaxially grown on GaAs or Ge substrates [14, 15]. Unfortunately, monolithically-integrated MJ devices often constrain the material choice to lattice-matched alloys and require current matching of the included junctions; the latter constraint further restricts the materials used and increases their sensitivity to changes in the solar spectrum as occur innately during the course of the day. Ideally, one would use separate junctions with independent contacts to harvest different parts of the solar spectrum. An ideal MJ device might therefore have three or four (or even more [16]) rather than two contacts, allowing the current and voltage of the individual junctions to be optimized independently.

One of the major problems with multi-terminal MJ photovoltaics is how to split the solar spectrum to illuminate the different junctions with different portions of the spectrum appropriate to the bandgap of the individual subcells. One example employs a mechanically-integrated tandem stack in which subcells with individual contacts are bonded by insulating adhesives [17–20]. This configuration, however, may require complicated back contact grid processing, or epitaxy of a highly conductive wide bandgap layer for lateral current transport, both of which remain technological challenges [6, 21–24]. Splitting of the solar spectrum, therefore, is more frequently done with a beam splitting element (dichroic/interference [16, 25], rugate [26], diffractive [27, 28] or dispersive [29]) while the concentration of light is done separately with a lens [30] or mirror [31]. This approach, while bearing great promise of achieving ultra-high efficiencies [32], has two disadvantages: the complexity of the beam splitting and lens optics, and limited transmission or reflection in the individual optical elements. In addition, beam splitting elements are generally angle-sensitive and impose a practical limit on the range of acceptance/exit angles within which the concentrators operate, which in turn significantly constrains the concentration ratios to values far below 1000X. Finally, chromatic aberration is an intrinsic feature of all lenses that limits the ability of conventional concentrators to provide a spectrally uniform illumination on a photovoltaic device [33, 34].

Here, we propose, model, and demonstrate a proof of concept for a solar concentrator combined with a spectrum splitter based on using chromatic aberration to produce both the focusing and the spectrum splitting in one optical element. The demonstration includes the use of a four-terminal two-junction photovoltaic collector with which we present data on optimization of the placement of the two photovoltaic junctions relative to the focusing lens. Our results show that a spectral separation with controlled optical loss can be realized by proper design of the solar converters. Ultra-high concentration is inherent in this architecture, making it a potential compact/low-cost candidate for bettering the full spectrum utilization of solar energy.

Methods

Fabrication of InGaP and GaAs solar microcells

Details can be found in supporting documents S2 and S3, available online at stacks.iop.org/JOPT/20/06LT01/mmedia.

InGaP/GaAs and InGaP/InGaP device integration

The GaAs microcell device on glass with thin adhesive (NOA61, Norland Products) was aligned and bonded to the rear glass surface of an InGaP microcell using a mask aligner and subsequent photocuring. Fabrication of the lower InGaP solar microcell in the InGaP/InGaP device followed the procedures in S3 and the wet etching recipes in S2. The InGaP/InGaP integration is the same as described for InGaP/GaAs device.

Device characterization

The device was mounted on a home-made positional irradiance measurement system (PIMS) which consists of three linear and one rotational stages. The photovoltaic characteristics were measured using a source meter (Keithley 2440 SMU) and a 1000 W full spectrum xenon arc lamp solar simulator (ABET Sun 2000). A custom-made broadband mirror was used to guide the beam across the room to the PIMS, where the irradiance was calibrated to be 37.88 mW cm^{-2} based the J_{sc} of the InGaP subcell in the InGaP/GaAs device. Ray tracing simulations in figures 4(b) and (c) were corrected for the spectral irradiance and 1.3° half-angle divergence of the solar simulator, actual contact shading and effective area of the subcells, as well as the fill factors of the microcells measured at similar current densities.

Numerical analysis

Bulk dielectric materials obey normal dispersion in which refractive index decreases with increasing wavelength. In optics, this phenomenon gives rise to the chromatic aberration of a lens, with a short focal length for the 'blue photons' and a longer one for the 'red'. To understand how this phenomenon can be used for spectrum splitting, two proxy subcells (InGaP, GaAs) are chosen to examine the effect, as illustrated in figure 1(a). Here, the cells are separated by a distance corresponding to a difference in focal length: the InGaP subcell closer to the lens has a wide bandgap (1.88 eV) to collect the blue photons while the GaAs subcell further along the optical axis has a narrower bandgap (1.41 eV) to collect the red photons.

To numerically model the system, we consider a transparent thin lens with a radius of R, in which the lensmaker equation holds for the relevant spectrum (300–900 nm):

$$\frac{1}{f(\lambda)} = [n(\lambda) - 1]\left[\frac{1}{R_1} - \frac{1}{R_2}\right],$$

where $f(\lambda)$ is its focal length, $n(\lambda)$ is the refractive index of the lens material, and R_1 and R_2 are the radii of curvature of the lens surfaces. Dividing $f(\lambda)$ by a focal length of a specific wavelength (here, we use the Fraunhofer D-spectral line with $f_0 \equiv f(589\text{ nm})$, $n_0 \equiv n(589\text{ nm})$) yields a normalized focal length that depends only on the refractive index of the lens material according to:

$$f(\lambda)/f_0 = \frac{n_0 - 1}{n(\lambda) - 1}.$$

Two circular subcells (InGaP with a radius r at a distance z and GaAs) are placed along the optical axis to collect the split illumination from the collimated beam normal to the lens. For the GaAs cell, its size is not specified but assumed to be large enough to collect all the rays that have a focal length longer than z and that pass by the edges of the InGaP subcell. We assume the InGaP subcell is opaque on the rear terminus (equivalent to full back metallization) to differentiate the design from traditional tandem stacks, in which the top subcell is optically transparent to the bottom subcell (a design that requires either complicated back contact grids or growth of a wide bandgap lateral conduction layer, as are discussed in the introduction section).

An analysis based on geometrical optics (see table S1.1 for details) shows that the optical efficiencies of the subcells, $OE_{\mathrm{InGaP}}(\lambda)$ and $OE_{\mathrm{GaAs}}(\lambda)$ (defined as the fraction of light at a certain wavelength that falls onto a specific subcell), are governed by three parameters: (a) $n(\lambda)$; (b) normalized InGaP subcell position z/f_0; and (c) the InGaP geometric concentration factor R^2/r^2. Figure 1(b) shows a numerical simulation of the optical efficiencies for the system using: (a) dense flint glass material, SF5; (b) $z/f_0 = 0.9637$; and (c) $R^2/r^2 = 4289$, where the sharp spectral cutoff occurs at ~520 nm. Two notable optical losses are evident in the plot, each occurring at the two ends of the InGaP absorption window. At the high-energy end, part of the UV photons (below 420 nm) are lost due their short focal length, making the beam diverge before reaching the InGaP cell. At the low-energy end, red photons incident on the InGaP cell are not transmitted to the GaAs subcell for photovoltaic conversion due to its opacity in this frequency range. In addition, a voltage loss exists when the GaAs subcell absorbs photons with energies higher than the InGaP band edge (i.e., photons below 660 nm).

The two loss avenues (optical, voltage) mentioned above actually correspond to two attributes that underlie a good spectrum splitting system: (1) high overall optical efficiency and (2) sharp spectral band separation at the desired band edge. These two attributes can be gauged together by measuring the proportion of light that falls to a subcell with a matching bandgap, defined as the spectral separation factor (SSF) by the following equation:

$$\mathrm{SSF} = \frac{\int_{300\text{ nm}}^{660\text{ nm}} OE_{\mathrm{InGaP}}(\lambda;\, n,\, z/f_0,\; R^2/r^2)\,\mathrm{d}\lambda + \int_{660\text{ nm}}^{880\text{ nm}} OE_{\mathrm{GaAs}}(\lambda;\, n,\, z/f_0,\; R^2/r^2)\,\mathrm{d}\lambda}{\int_{400\text{ nm}}^{880\text{ nm}} 1\,\mathrm{d}\lambda},$$

where 660 and 880 nm correspond to the absorption cutoffs of the InGaP and GaAs solar cells. 'Perfect' spectrum splitting corresponds to an SSF value of 1, while a homogenous spectral distribution with unit transmittance corresponds to an SSF value of 0.5. Modeling was carried out to optimize the refractive index $n(\lambda)$ and geometric parameters (z/f_0 and R^2/r^2) with respect to SSF, as shown in figures 2(a)–(c). The

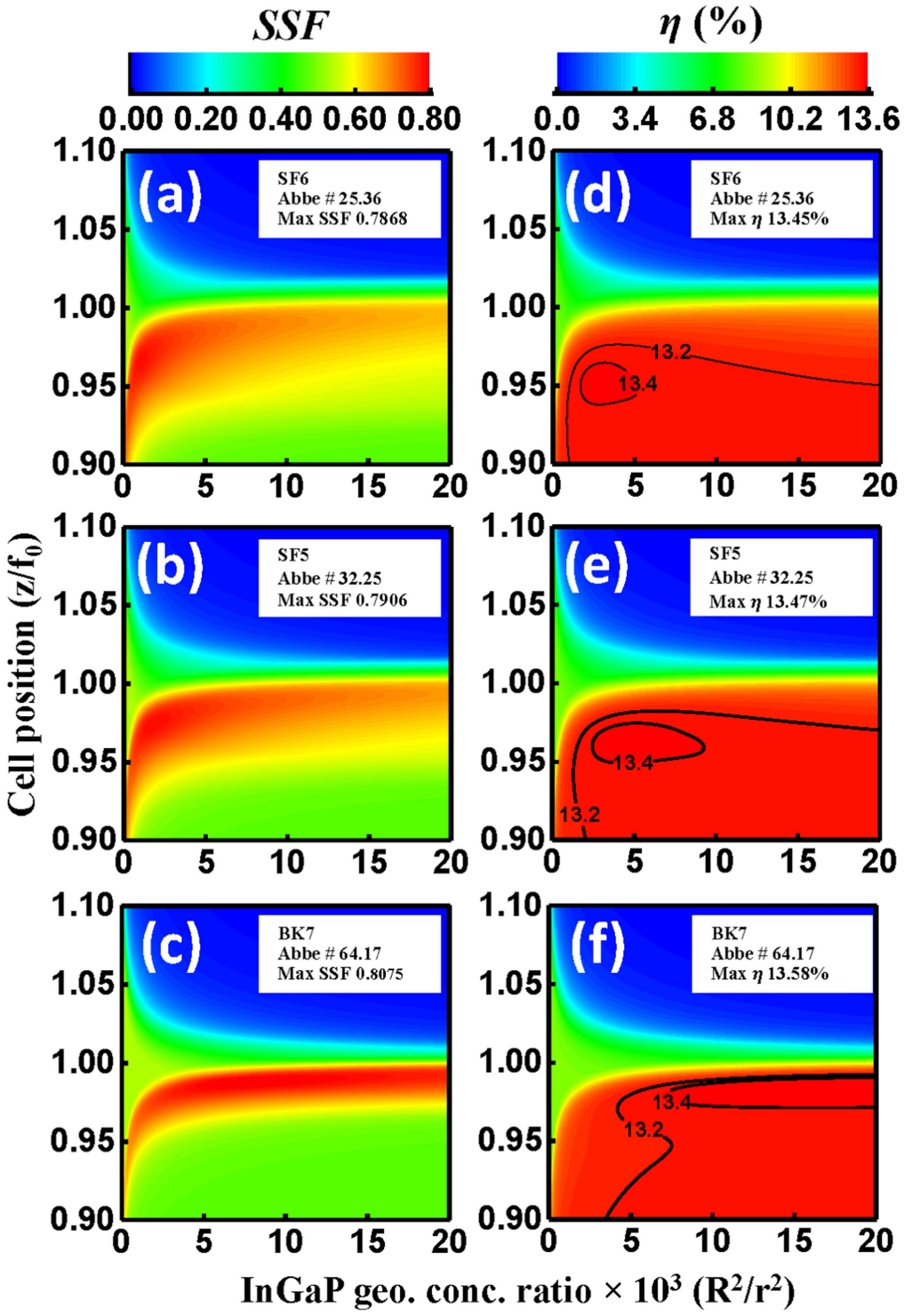

Figure 2. Contour plots of the spectral separation factor (SSF) and energy conversion efficiency (η) for three glass materials SF6 (a), (d), SF5 (b), (e) and BK7 (c), (f) as a function of the InGaP cell position z/f_0 and geometric concentration factor R^2/r^2. The contour lines ($\eta > 13.2\%$) in plots (d)–(f) encircle the configuration space where reduced thermoloss, resulting from spectral band separation, compensates the optical loss and creates a net positive efficiency boost compared to the unintegrated GaAs subcell ($\eta = 13.2\%$). A high InGaP geometric concentration ratio (>2000X) and precise spatial positioning (within 5% of the focal length f_0) are required for highly efficient power generation.

SSF for three different common glass materials (dense flint glass SF5, SF6, and borosilicate crown glass BK7) with different dispersion properties (denoted by Abbe number, a smaller Abbe number corresponding to higher dispersion, see figure S1.1) can all be optimized to near 0.8 by tuning the InGaP cell position z/f_0 (within 5% of the focal length) and geometric concentration factor R^2/r^2. The result shows that the system can indeed act as an effective spectrum splitter, though not an ideal one (SSF < 1).

The total energy conversion efficiency (η) under the AM 1.5 D solar spectrum for the above-mentioned lens materials with different dispersion properties are also calculated as a

function of z/f_0 and R^2/r^2:

$$\eta = \frac{V_{oc} \cdot FF \cdot q \cdot \int \Phi \cdot EQE \cdot OE \, d\lambda}{\int \Phi \cdot \frac{hc}{\lambda} d\lambda},$$

where Φ is the spectral photon flux, *EQE* the measured external quantum efficiency of the two proxy solar microcells (see figure 4(a) or supplementary materials S2 and S3), and h, c, and q are Planck's constant, the speed of light and the electron charge, respectively. The 1 sun values (see figures 3(b) and (c)) of the open-circuit voltage, V_{oc}, and fill factor, FF, were used in all cases so that the calculated efficiency gain benefits only from the spectrum splitting but not optical concentration. The contour maps in figures 2(d)–(f) illustrate the η values as a function of z/f_0 and R^2/r^2 for all three glass materials. Notice that the SSF map does not strictly align with the η map because the *EQE*s of the subcells are not perfect step functions, and thus different irradiance weight of the solar spectrum differentiates the η map from the SSF map. The contour lines highlighted on the η maps encircle the configuration space where the η exceeds the individual efficiencies of the unintegrated InGaP (8.72%) or GaAs (13.2%) subcell. Marginal efficiency enhancements resulting from the spectral band redistribution were achieved (by 0.2%–0.4%) for the three glasses under consideration. The contour map shows that a high efficiency system necessitates a high InGaP geometric concentration ratio as well as precise spatial positioning (i.e. z/f_0) of the subcell. It is interesting that the maximum efficiencies (η_{max}) obtainable for these glass materials are very similar (13.45%–13.58%, shown in the inset box) regardless of the degrees of dispersion of the materials. Even though the InGaP concentration ratios (R^2/r^2) required for efficient spectrum splitting vary with different materials, they all lie in the ultra-high concentration (>2000X) region where conventional spectrum splitting optics are rarely used. For practical reasons, highly dispersive materials are preferred because they require a lower and more practical R^2/r^2.

Proof-of-concept demonstration

To demonstrate the concept in a realistic setting, we employed a commercial aspheric plano-convex lens (Edmund Optics, Ø 15 mm, effective focal length 9 mm) made of the highly dispersive material, SF5. Test InGaP (1.88 eV) and GaAs (1.41 eV) microcells were prepared with optimized lateral dimensions of 400 × 400 μm^2 and 650 × 650 μm^2, respectively (see ray tracing in figure S1.2). The detailed process flow and cell performance data are documented in the supporting information S2 and S3. In brief, the solar microcells were first fabricated on chip by the standard microfabrication processes. Using techniques of epitaxial lift-off [35, 36] and transfer-printing [37, 38], the microcells were subsequently integrated onto a glass substrate with patterned metal filament electrodes, as shown in figure 3(a). Their experimental 1 sun and 250 sun *J*–*V* performances under a simulated AM 1.5 G solar spectrum are plotted in figures 3(b) and (c). Even though the microcells suffer from parasitic resistance under high current densities, fill factors are maintained above 0.7 up to 250X. The two subcells were subsequently stacked together using an index-matched optical adhesive with an optimized

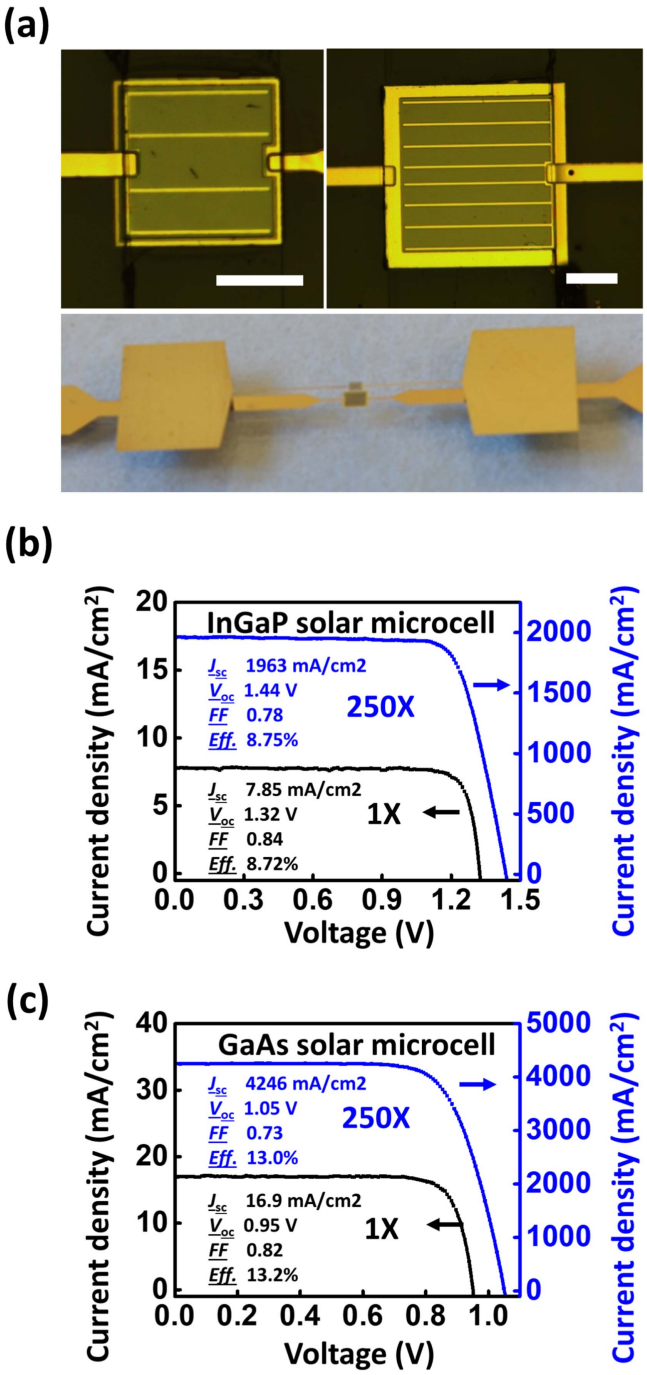

Figure 3. (a) Optical images of the four-terminal two-junction photovoltaic collector. The upper images show the InGaP (left) and GaAs (right) subcells mounted on 1 mm thick soda lime glass. The scale bars are 200 μm in length. The lower image shows the mechanically stacked InGaP/GaAs device. *J*–*V* characteristics and schematic illustrations are shown for (b) the InGaP and (c) the GaAs subcells under 1X and 250X concentrations calculated based on the active absorbing area of the microcells.

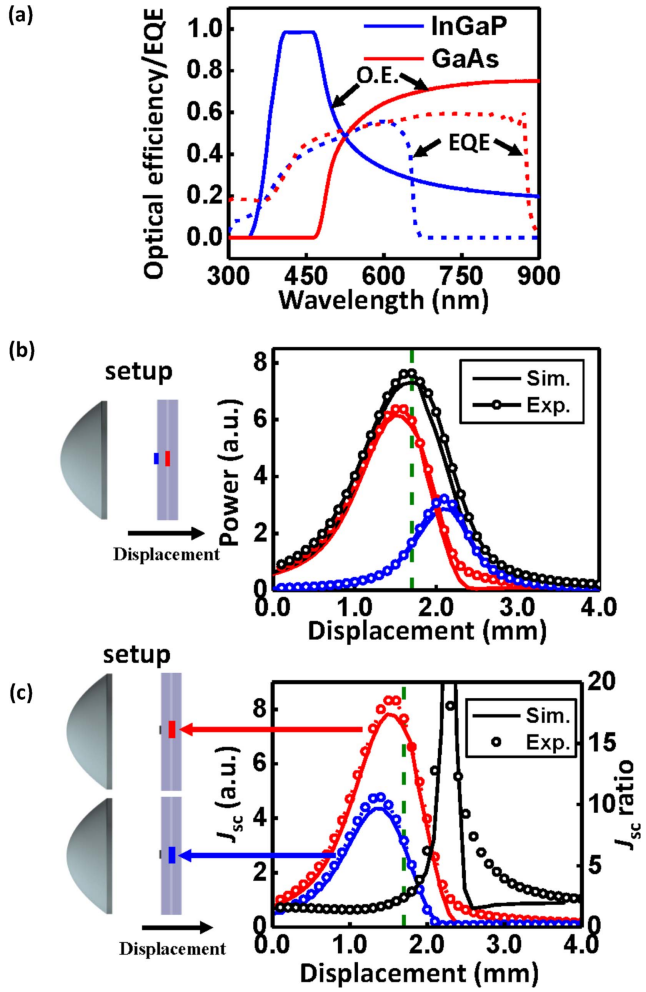

Figure 4. (a) Simulated photon flux densities on the InGaP and GaAs subcells given the incident AM 1.5 D spectrum. The corresponding InGaP geometric concentration ratio is 1104, and the SSF is calculated to be 0.59. (b) Power output of the InGaP/GaAs device as it moves along the optical axis, with larger displacements corresponding to greater distances from the lens as indicated by the cartoon in the inset box. The blue lines and red lines represent power outputs from the InGaP and the GaAs subcell respectively, while the black lines represent the total output. The green dashed line highlights the optimum position (displacement = 1.7 mm) where the total power output is greatest. (c) Comparison of the J_{sc} of the lower subcells for the two device configurations, i.e. InGaP/GaAs (red) and InGaP/InGaP (blue). Different peak positions conform to dispersion along the optical axis. The J_{sc} ratio (black) increased from 1.5 to 2.4 at the optimum position (displacement = 1.7 mm), demonstrating the lower subcell receives a spectrum which has a heavier weight on its red end.

spatial gap of 1 mm (see ray tracing in figure S1.2), whose photo image is shown in the lower panel of figure 3(a).

The geometric concentration relative to the InGaP subcell is 1104X, lower than the simulated optimum (>2000X). Assuming an incoming radiation that matches the AM 1.5 D solar spectrum with a divergence half-angle of 0.25° and no Fresnel losses on all interfaces, the incident photon flux densities on the two subcells were determined by ray tracing (LightTools, Synopsys), as shown in figure 4(a) together with the *EQE*s of the two subcells. The spectral separation is evident in the plot, with a computed SSF of 0.59. The relatively limited SSF value is due to optical losses associated with the low concentration factor, as some low-energy photons spanning from 660 to 800 nm (9% of the photon flux between 300 and 900 nm) are blocked by the InGaP subcell. Other factors, including tracking errors and non-ideal light sources (i.e. divergence angle larger than 0.25°) will further decrease SSF (see figures S1.3 and S1.4).

The optimum placement of the four-terminal two-junction photovoltaic collector relative to the lens is determined by scanning the device along the optical axis until maximum power output is read. This is accomplished by illuminating the device with a simulated AM 1.5 D spectrum on a custom-made PIMS [39] which is comprised of four motorized stages to provide precise control of the displacement of the device, defined as the distance between the InGaP cell and a fixed position along the optical axis. (A larger displacement corresponds to a greater distance of the device from the lens.) Figure 4(b) shows the power output of the device as it moves along the optical axis by a step distance of 0.1 mm. The power output for the GaAs and InGaP subcells peaks at displacements of 1.5 mm and 2.1 mm, respectively, whereas the optimum displacement is found to be 1.7 mm. The experiment results agree very well with the simulations, with corresponding peaks appearing at nearly identical displacements.

To locally detect the spectral separation at the focal point, an InGaP/InGaP mechanically stacked device was prepared. It resembles the InGaP/GaAs counterpart except that the lower subcell is replaced by an InGaP subcell with identical lateral dimensions. Figure 4(c) shows a comparison of the J_{sc} of the lower subcells for these two devices as a function of displacement. Their distinct J_{sc} peak positions further confirm the spectrum splitting effect. Given that the SSF value is not easy to obtain experimentally, we use instead the J_{sc} ratio between the two bottom subcells (GaAs to InGaP) to evaluate the degree of spectral separation. A higher J_{sc} ratio indicates a higher current in the GaAs device due to an incident spectrum with more red photons on the lower subcell. As a reference, the J_{sc} ratio between the unintegrated GaAs and InGaP subcells is 1.4 under the simulated AM 1.5 D solar spectrum. In the range of small displacement (<1.3 mm, i.e. the stacked subcells are very close to the lens), the J_{sc} ratio (~1.5) remains close to the reference value, indicating that the lower subcells in the two device configurations receive similar spectra. However, at a displacement of 1.7 mm, where the maximum power output occurs for the InGaP/GaAs device, the current ratio increased to 2.4, indicating effective spectrum splitting. The experimental J_{sc} ratios match well with those calculated by ray tracing, which predicts an SSF of 0.57 at the optimum displacement (see figure S1.5).

The experiment successfully demonstrates that the lens projects an inhomogeneous spectrum along the optical axis. At the designed maximum power output placement, the photovoltaic collector receives a spectrum that has a heavier weight on its red end in the lower subcell. The close

alignment of experimental and simulated data validates the simulation results showing that a concentrator and spectrum splitter can be combined in one optical element.

The architecture reported here differs from the otherwise similar mechanical stacks (which also provide multiple terminals but require sub-bandgap transmission of the top junction) by its unique potential of inclusion of a back metallic reflector to each junction. It has been known that the back reflector can significantly boost the V_{oc} of the device by recycling luminescent photons. More importantly, it potentially enables far better electrical and thermal management to the device operating at high concentration values. Series resistance is perhaps the single most important factor that limits CPV from achieving even higher optical concentrations. Even the best cells available today see a roll-off in the fill factor at a few hundred suns due to the series resistance. A fully metalized surface, however, provides the best electrical contacts that affords the use of the high concentration that would otherwise be extremely challenging for mechanically stacked cells. A back mirror also greatly facilitates heat transfer, another factor that deserves careful evaluation in the design of CPV systems. In principle, this simple architecture can support additional bandgaps and spectral bands for further improvement. We also note that photonic designs, such as subwavelength gratings, could be employed directly on the lens to facilitate frequency-selective splitting. The multi-terminal MJ cell configuration supported by this concentrator also provides a platform for the deployment of the most advanced MJ cell designs that employ air gaps or selective mirrors for efficient photon recycling and radiative coupling [10, 40]. These benefits, however, must be weighed against the shadow loss brought about by the top junction and the consequent requirements for fully optimized cells that are required to support operation at high levels of optical concentration.

Conclusion

We demonstrate a proof-of-concept concentrator that produces both focusing and spectrum splitting in one optical element based on the chromatic aberration of a lens. The conceptual framework is simple, and a numerical model has been proposed to describe its essential operational properties. A four-terminal two-junction photovoltaic collector was prepared following this design rule using epitaxial lift-off and transfer-assembly techniques. Preliminary experimental results show the spectral band separation to be in close agreement with the simulation, confirming the proposed architecture as a viable spectrum splitting system for high concentration applications.

Acknowledgments

This work is part of the 'Light-Material Interactions in Energy Conversion' Energy Frontier Research Center funded by the US Department of Energy, Office of Science, Office of Basic Energy Sciences under Award Number DE-SC0001293. The authors thank C Corcoran and M Meitl for early discussions on solar cell design and fabrication processes.

ORCID iDs

R G Nuzzo https://orcid.org/0000-0003-2310-2045

References

[1] De Vos A 1980 Detailed balance limit of the efficiency of tandem solar cells *J. Phys. D: Appl. Phys.* **13** 839
[2] Luque A 1993 Coupling light to solar cells *Advances in Solar Energy* (Boulder, CO: American Solar Energy Society, Inc.)
[3] King R R 2008 Multijunction cells—record breakers *Nat. Photon.* **2** 284
[4] Dimroth F and Kurtz S 2007 High-efficiency multijunction solar cells *MRS Bull.* **32** 230
[5] Tobias I and Luque A 2002 Ideal efficiency of monolithic, series-connected multijunction solar cells *Prog. Photovolt.* **10** 323
[6] Cotal H, Fetzer C, Boisvert J, Kinsey G, King R, Hebert P, Yoon H and Karam N 2009 III–V multijunction solar cells for concentrating photovoltaics *Energy Environ. Sci.* **2** 174
[7] Miller O D, Yablonovitch E and Kurtz S R 2012 Strong internal and external luminescence as solar cells approach the Shockley–Queisser limit *IEEE J. Photovolt.* **2** 303
[8] Schnitzer I, Yablonovitch E, Caneau C and Gmitter T J 1993 Ultrahigh spontaneous emission quantum efficiency, 99.7% internally and 72% externally, from AlGaAs/GaAs/AlGaAs double heterostructures *Appl. Phys. Lett.* **62** 131
[9] Sheng X *et al* 2015 Device architectures for enhanced photon recycling in thin-film multijunction solar cells *Adv. Energy Mater.* **5** 1400919
[10] Eisler C N, Abrams Z R, Sheldon M T, Zhang X and Atwater H A 2014 Multijunction solar cell efficiencies: effect of spectral window, optical environment and radiative coupling *Energy Environ. Sci.* **7** 3600
[11] Kosten E D, Atwater J H, Parsons J, Polman A and Atwater H A 2013 Highly efficient GaAs solar cells by limiting light emission angle *Light Sci. Appl.* **2** e45
[12] Green M A, Emery K, Hishikawa Y, Warta W and Dunlop E D 2016 Solar cell efficiency tables (version 48) *Prog. Photovolt.* **24** 905
[13] Leite M S, Woo R L, Munday J N, Hong W D, Mesropian S, Law D C and Atwater H A 2013 Towards an optimized all lattice-matched InAlAs/InGaAsP/InGaAs multijunction solar cell with efficiency >50% *Appl. Phys. Lett.* **102** 033901
[14] King R R, Law D C, Edmondson K M, Fetzer C M, Kinsey G S, Yoon H, Sherif R A and Karam N H 2007 40% efficient metamorphic GaInP/GaInAs/Ge multijunction solar cells *Appl. Phys. Lett.* **90** 183516
[15] Steiner M, Bösch A, Dilger A, Dimroth F, Dörsam T, Muller M, Hornung T, Siefer G, Wiesenfarth M and Bett A W 2015 FLATCON® CPV module with 36.7% efficiency equipped with four-junction solar cells *Prog. Photovolt., Res. Appl.* **23** 1323
[16] Eisler C N, Kosten E D, Warmann E C and Atwater H A 2013 Spectrum splitting photovoltaics: polyhedral specular reflector design for ultra-high efficiency modules *39th IEEE Photovoltaic Specialists Conf.* p 1848

[17] Mathews I, O'mahony D, Thomas K, Pelucchi E, Corbett B and Morrison A P 2015 Adhesive bonding for mechanically stacked solar cells *Prog. Photovolt.* **23** 1080
[18] Gee J M and Virshup G F 1988 A 31%-efficient GaAs/silicon mechanically stacked, multijunction concentrator solar cell *20th IEEE Photovoltaic Specialists Conf.* p 754
[19] Zhao L, Flamand G, Mols Y, Van Der Heide J and Poortmans J 2010 Novel mechanically stacked multi-junction solar cells applying ultra-thin III–V cells and wafer based germanium cell *ECS Trans.* **27** 1123
[20] Sheng X *et al* 2014 Printing-based assembly of quadruple-junction four-terminal microscale solar cells and their use in high-efficiency modules *Nat. Mater.* **13** 593
[21] Mcmahon W E *et al* 2013 Metal pillar interconnection topology for bonded two-terminal multijunction III–V solar cells *IEEE J. Photovolt.* **3** 868
[22] Adachi S 2009 *Properties of Semiconductor Alloys: Group-IV, III-V and II-VI Semiconductors* (New York: Wiley)
[23] Braun A, Vossier A, Katz E A, Ekins-Daukes N J and Gordon J M 2012 Multiple-bandgap vertical-junction architectures for ultra-efficient concentrator solar cells *Energy Environ. Sci.* **5** 8523
[24] Walsh A *et al* 2013 Limits to doping of wide band gap semiconductors *Chem. Mater.* **25** 2924
[25] Barnett A *et al* 2009 Very high efficiency solar cell modules *Prog. Photovolt., Res. Appl.* **17** 75
[26] Peters M, Goldschmidt J C, Loper P, Gross B, Upping J, Dimroth F, Wehrspohn R B and Blasi B 2010 Spectrally-selective photonic structures for PV applications *Energies* **3** 171
[27] Gordon M, Zhang D, Vorndran S, Russo J M, Luscombe C K, Shaheen S E and Kostuk R K 2012 Planar holographic spectrum-splitting PV module design *Proc. SPIE* **8468** 846808
[28] Escarra M D, Darbe S, Warmann E C and Atwater H A 2013 Spectrum-splitting photovoltaics: holographic spectrum splitting in eight-junction, ultra-high efficiency module *39th IEEE Photovoltaic Specialists Conf.* p 1852
[29] Stefancich M, Zayan A, Chiesa M, Rampino S, Roncati D, Kimerling L and Michel J 2012 Single element spectral splitting solar concentrator for multiple cells CPV system *Opt Express* **20** 9004
[30] Luque A L 2007 *Concentrator Photovoltaics* (Berlin: Springer)
[31] Welford W T and Winston R 1978 The optics of nonimaging concentrators *Light and Solar Energy* (New York: Academic)
[32] Polman A and Atwater H A 2012 Photonic design principles for ultrahigh-efficiency photovoltaics *Nat. Mater.* **11** 174
[33] Garcia I, Espinet-Gonzalez P, Rey-Stolle I and Algora C 2011 Analysis of chromatic aberration effects in triple-junction solar cells using advanced distributed models *IEEE J. Photovolt.* **1** 219
[34] Kurtz S R and Neill M J O 1996 Estimating and controlling chromatic aberration losses for two-junction, two-terminal devices in refractive concentrator systems *25th IEEE Photovoltaic Specialists Conf.* p 361
[35] Yablonovitch E, Hwang D, Gmitter T, Florez L and Harbison J 1990 Van der Waals bonding of GaAs epitaxial liftoff films onto arbitrary substrates *Appl. Phys. Lett.* **56** 2419
[36] Cheng C-W, Shiu K-T, Li N, Han S-J, Shi L and Sadana D K 2013 Epitaxial lift-off process for gallium arsenide substrate reuse and flexible electronics *Nat. Commun.* **4** 1577
[37] Meitl M A, Zhu Z T, Kumar V, Lee K J, Feng X, Huang Y Y, Adesida I, Nuzzo R G and Rogers J A 2006 Transfer printing by kinetic control of adhesion to an elastomeric stamp *Nat. Mater.* **5** 33
[38] Sheng X, Corcoran C J, He J, Shen L, Kim S, Park J, Nuzzo R G and Rogers J A 2013 Enhanced ultraviolet responses in thin-film InGaP solar cells by down-shifting *Phys. Chem. Chem. Phys.* **15** 20434
[39] Flowers C A, Darbe S, Eisler C N, He J and Atwater H A 2014 Positional irradiance measurement: characterization of spectrum-splitting and concentrating optics for photovoltaics *Proc. SPIE* **9175** 91750F
[40] Ganapati V, Ho C S and Yablonovitch E 2015 Air gaps as intermediate selective reflectors to reach theoretical efficiency limits of multibandgap solar cells *IEEE J. Photovolt.* **5** 410